Applied Catalysis B: Environmental 324 (2023) 122290

Contents lists available at ScienceDirect

Applied Catalysis B: Environmental

journal homepage: www.elsevier.com/locate/apcatb

Mechanochemical localization of vanadia on titania to prepare a highly sulfur-resistant catalyst for low-temperature NH_3-SCR

Keon Ha Hwang [a], Namjun Park [a], Hwangho Lee [a], Kyung-Min Lee [b], Se Won Jeon [a], Hyun Sub Kim [a], Yongkyu Lee [a], Tae Jin Kim [b], Won Bo Lee [a], Do Heui Kim [a,*]

[a] School of Chemical and Biological Engineering, Institute of Chemical Processes, Seoul National University, 1 Gwanak-ro, Gwanak-Gu, Seoul 08826, Republic of Korea
[b] Department of Materials Science and Chemical Engineering, Stony Brook University, Stony Brook, NY 11794, USA

ARTICLE INFO

Keywords:
NH_3-selective catalytic reduction
V_2O_5/WO_3-TiO_2
Ammonium bisulfate deposition
Density functional theory
Vanadia localization

ABSTRACT

This paper reports a novel attempt to mechanochemically localize vanadia on the surface of WO_3-TiO_2 by physically grinding high-vanadia-loading V_2O_5/WO_3-TiO_2 with WO_3-TiO_2. On the surface of the vanadia-localized catalysts, clustered vanadia sites exhibited enhanced activity for low-temperature (< 250 °C) NH_3-selective catalytic reduction (NH_3-SCR) by forming polymeric structures. The catalyst with localized vanadia simultaneously exhibited superior sulfur resistance, which has not been achieved in conjunction with high activity via conventional synthesis. Mechanochemical interactions between clustered vanadia and titania resulted in the formation of TiO_2 sites adjacent to the vanadyl species without deforming the polymeric structure of the vanadia. Density functional theory calculations showed that ammonium bisulfate (ABS) was considerably more stable in the presence of exposed TiO_2 adjacent to the vanadyl species. The exposed TiO_2 sites absorbed the deactivating material ABS from the clustered vanadia sites, which prevented the blockage of the catalytic active sites, leading to less deactivation.

1. Introduction

Nitrogen oxides (NO_x), which are well-known causes of smog, acid rain, and respiratory problems, can be efficiently removed from exhaust gas by an aftertreatment process involving selective catalytic reduction with NH_3 (NH_3-SCR) [1]. V_2O_5-WO_3/TiO_2 catalysts are predominantly used for NH_3-SCR in real-world applications owing to their high SCR activity and superior sulfur resistance above 300 °C [2]. Other potential NH_3-SCR catalysts, such as Mn oxides and Cu-zeolites, are susceptible to severe poisoning by the sulfur in the exhaust gas [3–7]. Thus, vanadia-based catalysts remain the only feasible option for the aftertreatment of sulfur-containing gases.

In an industrial plant, the exhaust gas cools down to 200 °C or lower when it reaches the SCR system, which is conventionally placed at the tail-end configuration of the entire setup [8,9]. These low exhaust temperatures cause two possible problems for vanadia-based catalysts. First, because conventional V_2O_5-WO_3/TiO_2 catalysts exhibit inferior NO_x removal ability at temperatures below 300 °C, the reactor is reheated to the operating temperature to provide sufficient thermal energy for activating the catalyst. This process results in unwanted fuel consumption and emission of greenhouse gases, which are highly undesirable from economic and environmental viewpoints [10]. Second, SO_2 poisoning can be induced by the ammonium bisulfate (ABS; $(NH_4)HSO_4$) produced at these temperatures. ABS is formed via the reaction between SO_3, H_2O, and NH_3. SO_3 is either present in the exhaust gas or is formed via the oxidation of SO_2 over V_2O_5-WO_3/TiO_2 catalysts [11,12]. At temperatures below 300 °C, the ABS salt is readily formed as a condensed, sticky liquid that physically blocks the pores and active sites of vanadia, thereby degrading its catalytic performance [8]. Because vanadia species are the main active sites for the oxidation of SO_2 to SO_3, ABS formation is inevitable in vanadia catalysts [13]. Therefore, developing V_2O_5-WO_3/TiO_2 catalysts with high NH_3-SCR activity and sulfur resistance in the low-temperature range (< 250 °C) have been of strong interest, which is the range that the present study focuses on.

The volatility of vanadium and tungsten or its derivatives on the catalysts is also of concern in the industry [14]. It may cause catalytic deactivation in the prolonged reaction period by agglomeration or loss of active catalytic sites. More importantly, the sublimated species may be released into the atmosphere, potentially harming human health and the environment [14]. However, the release of vanadium and tungsten

* Corresponding author.
E-mail address: dohkim@snu.ac.kr (D.H. Kim).

https://doi.org/10.1016/j.apcatb.2022.122290
Received 22 October 2022; Received in revised form 6 December 2022; Accepted 11 December 2022
Available online 20 December 2022

begins at high temperature of 500 °C and increases exponentially with temperature in commercially available V_2O_5-WO_3/TiO_2 catalysts [15]. Therefore, the impact of volatilization of vanadium and tungsten can be minimized in low-temperature NH_3-SCR under 250 °C [15].

The low-temperature SCR with V_2O_5-WO_3/TiO_2 creates a major dilemma in terms of selecting between the SCR activity and sulfur resistance, which are dependent on the vanadia loading. At low temperatures, catalysts with lower vanadia loadings (that is, 1 or 2 wt%) show high resistance to sulfur poisoning but exhibit relatively low SCR activities. The low surface density of vanadia results in isolated monomeric structures that do not exhibit high activity in low-temperature SCR [16,17]. In contrast, a higher vanadia content leads to high SCR activity even at low temperatures by forming highly active polymeric vanadyl structures; however, it makes the catalyst severely vulnerable to sulfur [13,16]. Because the use of vanadia must be minimized considering its biotoxicity, attempts have been made to enhance the SCR activity of low-vanadia-content catalysts by impregnating new materials [18–23] or using different synthesis methods [24,25], while maintaining a high sulfur resistance. However, strategies such as introducing new materials and using complicated synthesis methods have problems such as high ingredient costs and difficulty in regeneration, which make the catalyst economically demanding.

Mechanochemical synthesis—a seemingly simple approach—has attracted considerable attention for enabling certain characteristic features that are impossible to realize via solution-based synthesis[26–31]. Previous studies from our group have provided new insights into mechanochemical synthesis for low-temperature SCR; for instance, the sulfur resistance of vanadia catalysts was enhanced by physically mixing heterogeneous catalysts such as zeolite or alumina [32–34]. Additionally, liquid-phase ABS was found to migrate to the physically mixed catalysts, thereby protecting the vanadia active sites from physical deactivation [32–34].

In this regard, a cost-effective yet simple strategy was devised in the present study to enhance both the SCR activity and sulfur resistance at low temperatures using a mechanochemical method, which enabled the localization of vanadia on the WO_3-TiO_2 support. The catalysts with highly localized surface vanadia combine the advantages of low- and high-vanadia-content catalysts, providing new insight into the complex dilemma of the effect of vanadia loading on the SCR activity and sulfur resistance. This novel approach requires no extra materials or complicated synthesis methods, and thus provides practical advantages in the preparation of industrial NH_3-SCR catalysts. Moreover, these findings provide a fundamental understanding of the sulfur poisoning of the V_2O_5-WO_3/TiO_2 catalysts.

2. Experimental

2.1. Catalyst preparation

A V_2O_5/WO_3-TiO_2 catalyst containing 2 wt% V_2O_5 (denoted as 2 V/DT-52; DT-52 = WO_3-TiO_2 with 7.7 wt% tungsten; TRONOX) was synthesized using a conventional wetness impregnation method. To this end, a vanadium precursor solution was initially prepared by dissolving ammonium metavanadate (Sigma Aldrich) in an oxalic acid solution (Sigma Aldrich) at a molar ratio of 1:1.2, and the resulting solution was stirred for one day at room temperature. A calculated amount of DT-52 was added as a support to the vanadium precursor solution and stirred for 3 h. The solution with DT-52 support was dehydrated using a rotary evaporator with a water bath at 80 °C and then completely dried overnight in an oven at 105 °C. The dried catalyst was calcined at 500 °C for 4 h at a heating rate of 10 °C/min. The resulting product was ground in a mortar for 5 min to obtain a homogeneous and fine powder. Other catalysts with different V_2O_5 contents (wt%) were synthesized according to the aforementioned protocol; these are denoted as 3 V/DT-52, 4 V/DT-52, 6 V/DT-52, and 8 V/DT-52. The compositions of the resulting *x*V/DT-52 catalysts were verified by inductively coupled plasma-atomic emission spectroscopy (ICP-AES) (Table S1).

To localize vanadia on the surface of DT-52 instead of dispersing it uniformly, 6 V/DT-52 and calcined DT-52 (500 °C for 4 h) were thoroughly mixed at a mass ratio of 1:2 and ground in a mortar for 10 min. The resulting mechanochemically synthesized V_2O_5/WO_3-TiO_2 catalyst containing 2 wt% V_2O_5 was denoted 2 V/DT-52 HL, indicating that the vanadia species were highly localized. The conditions under which DT-52 was precalcined were identical to those used for calcining 6 V/DT-52.

To compare the effects of the physical grinding, 6 V/DT-52 and calcined DT-52 were separately pelletized, sieved to 180–250-μm-sized particles, and then agitated by hand at a mass ratio of 1:2. The sieved particles of 6 V/DT-52 and calcined DT-52 differed in their color (brown and white, respectively), and physical contact between 6 V/DT-52 and calcined DT-52 was minimized. The loosely mixed sample is denoted as 6 V/DT-52 + DT-52 (1:2). The schemes for synthesizing 2 V/DT-52, 2 V/DT-52 HL, and 6 V/DT-52 + DT-52 (1:2) are illustrated in Fig. S1, for ease of comprehension.

The catalysts were impregnated with 1 wt% ABS to investigate its poisoning effect. The prefix "1ABS-" is used herein to denote the 1-wt%-ABS-impregnated catalysts. Impregnation was performed using the incipient wetness impregnation method, except for 2 V/DT-52 HL and 6 V/DT-52 + DT-52 (1:2), whose ABS-incorporated versions were prepared by pre-impregnating 6 V/DT-52 with ABS and following the subsequent steps, as mentioned above. This is because ABS is mainly formed on vanadia sites, as vanadia active sites are primarily responsible for SO_2 oxidation [13]. A negligible amount of ABS was formed on pure DT-52 after 10 h of SO_2 aging (Table S3). To normalize the ABS amount to 1 wt% of the total catalyst, 3-wt%-ABS-impregnated 6 V/DT-52 was used to prepare ABS-impregnated 2 V/DT-52 HL and 6 V/DT-52 + DT-52 (1:2).

For comparison purposes, 6 V/DT-52 was thoroughly mixed with fumed silica (Sigma Aldrich, surface area: 395 m^2/g) or DT-51 (TiO_2; TRONOX) at a mass ratio of 1:2, and the mixtures were ground in a mortar for 10 min; the resulting catalysts are denoted as 2 V/DT-52 HL-Silica and 2 V/DT-52 HL-DT-51, respectively. DT-51 was calcined at 500 °C for 4 h before mixing with 6 V/DT-52.

2.2. Catalyst characterization

The specific surface areas of the catalysts were obtained using the ASAP 2000 analyzer to acquire N_2 adsorption–desorption isotherms at 77 K and calculated using the Brunauer–Emmett–Teller (BET) method. ICP-AES was performed using an OPTIMA 8300 instrument (Perkin-Elmer) to determine the vanadium and tungsten contents of the synthesized catalysts. In situ Raman spectra were acquired using a BaySpecNomadicTM Raman spectrometer with a 532 nm laser. To remove moisture and impurities, the environmental cell (CCR1000, Linkam) was heated at 250 °C in a 3% O_2/Ar atmosphere for 30 min. Raman spectra of the dehydrated samples were collected under identical conditions. The acquisition time of each scan was 10 s, and the final spectrum was accumulated from 10 scans.

Experiments on temperature-programmed desorption (TPD) of NH_3 were conducted using a BELCAT II device (Microtrac MRB). To this end, the catalysts were pretreated at 350 °C in 5% O_2 balanced with He for 1 h and cooled to 100 °C in He. NH_3 adsorption was performed using 5% NH_3 balanced with He for 30 min, followed by exposure to He for 15 min. TPD was performed using He as a carrier gas from 100° to 550°C at a ramping rate of 10 °C/min, and the measurements were conducted using a thermal conductivity detector. In situ diffuse reflectance infrared Fourier transform spectroscopy (DRIFTS) profiles were obtained using a Fourier transform infrared (FT-IR) spectrometer (Nicolet 6700, Thermo Scientific) equipped with a DRIFTS cell (Praying Mantis, Harrick). For the NH_3 adsorption experiments, the sample packed in the DRIFTS cell was pretreated with 5% O_2 balanced with N_2 (100 mL/min) at 350 °C. After the pretreatment, the sample was cooled to 100 °C in N_2 and fully saturated with 500 ppm NH_3 balanced with N_2 for 1 h. The sample was

then exposed to N_2 for 30 min and measured.

The amount of sulfur deposited on the SO_2-poisoned catalysts was measured using a Flash 2000 instrument (Thermo Fisher Scientific). Cs-corrected transmission electron microscopy (TEM) images of the catalysts were obtained using the JEM-ARM200F device. Scanning electron microscopy (SEM) images of the catalysts were acquired using a JSM-7600 F instrument. Energy dispersive spectroscopy (EDS) was performed to investigate the distribution of elements in the SO_2-poisoned catalysts and to measure the dispersion of vanadia on them. Acetone was used as the solvent to disperse the catalysts on the TEM grid to prevent the dissolution of ABS and vanadia. TPD experiments on the ABS-impregnated and SO_2-poisoned samples were conducted using a mass spectrometry (MS) device (HIDEN Analytical Quantitative Gas Analysis (QGA)) with an SEM detector. The temperature was increased from 100° to 900°C at a ramping rate of 10 °C/min. The gas hourly space velocity (GHSV) of pure N_2 was 60,000 mL/h·g_{cat}.

2.3. Catalyst evaluation

All samples were pelletized and sieved to 180–250-μm-sized particles to prevent pressure drop. The NH_3-SCR activity was measured under the following conditions: 500 ppm NO, 600 ppm NH_3, 10% O_2, 5% CO_2, 10% H_2O, and balance N_2. The total flow rate was 200 mL/min, and the GHSV was 100,000 mL/h·g_{cat}. NO_x concentrations were measured using an NO_x chemiluminescence analyzer (42i High level, Thermo Scientific). NO_x conversion was calculated using Eq. (1).

$$NO_x conversion(\%) = \frac{[NO_x]_{in} - [NO_x]_{out}}{[NO_x]_{in}} \times 100(\%). \quad (1)$$

The SO_2 poisoning test was conducted at 220 °C under the following conditions: 500 ppm NO, 600 ppm NH_3, 10% O_2, 5% CO_2, 10% H_2O, 100 ppm SO_2, and balance N_2. The total flow rate was 200 mL/min, and the GHSV was 50,000 mL/h·g_{cat}. The initial NO_x conversion was measured when the conversion rate was completely stabilized without SO_2 flow. The samples were poisoned under the aforementioned conditions by adding SO_2 for 10 h. The final NO_x conversion was measured after flowing the gas without SO_2 for 30 min. The SO_2 deactivation rate was calculated using Eq. (2).

$$SO_2 deactivation rate(\%) = \frac{Initial NO_x conversion - Final NO_x conversion}{Initial NO_x conversion} \times 100(\%) \quad (2)$$

The activation energy and turnover frequency (TOF) were determined by performing the reaction under conditions of 500 ppm NO, 600 ppm NH_3, 10% O_2, 5% CO_2, 10% H_2O, and balance N_2. A GHSV of 600,000 mL/h·g_{cat} was used to ensure that the NO_x conversions were below 20% and circumvent the mass diffusion limitation. Arrhenius plots ($\ln(-r_{NO_x})$vs. $1/T$) were constructed by calculating the NO_x consumption rate using Eq. (3), in which γ_{NO_x} is the partial pressure of NO (0.0005), V_{tot} is 0.2 L/min, P is 1 atm, R is the gas constant, T is the ambient temperature, and W is the weight of the catalyst in the reactor (0.02 g).

$$-r_{NO_x} = \frac{NO_x conversion}{100} \bullet \gamma_{NO_x} \bullet \frac{V_{tot} \bullet P}{W \bullet R \bullet T} \quad (3)$$

TOFs were measured at 200 °C and calculated using Eq. (4), in which the NO_x consumption rate was divided by the number of vanadium species loaded on the catalyst, L is the V_2O_5 loading on the catalyst (wt %), and M is the molecular weight of V_2O_5 (181.88 g/mol).

$$TOF = -r_{NO_x} \bullet \frac{100 \bullet M}{2 \bullet L} \quad (4)$$

2.4. Computational details

Density functional theory (DFT) calculations of an ABS molecule and V_2O_5/WO_3-TiO_2 catalysts were conducted using the Vienna ab initio simulation package (VASP) [35] with the projector augmented-wave (PAW) pseudopotentials and generalized-gradient-approximation (GGA) functionals suggested by Perdew, Burke, and Ernzerhof (PBE) [36]. An energy cutoff of 500 eV was used, and spin polarization was considered for all catalyst calculations. The self-consistent field (SCF) convergence threshold was set with a convergence criterion of 10^{-6} eV. In the geometry optimizations, all structures were relaxed to the maximum force convergence criterion of 0.05 eV/Å.

A three-layer anatase TiO_2 (001) surface with a 3 × 3 surface unit cell (11.460 × 11.460 $Å^2$) and a 15-Å-thick vacuum layer along the z-axis were used. A total of 3 × 3 × 1 k-points were generated using the Monkhorst–Pack method. Vanadia species (VO_3 and V_2O_5), tungsten oxide (WO_3), and mixed species (VWO_5) were positioned on the top surface of TiO_2 to simulate the various loading states of the V_2O_5/WO_3-TiO_2 catalyst [37]. The bottom two layers were fixed, whereas the top layer, vanadia, tungsten oxide, and ABS were fully relaxed.

An isolated ABS molecule was investigated in a 20 × 20 × 20 $Å^3$ box with a gamma point located only in the Brillouin zone. The adsorption energy was calculated using Eq. (5).

$$E_{ads} = E_{catalyst+ABS} - \left(E_{catalyst} + E_{ABS}\right), \quad (5)$$

where $E_{catalyst+ABS}$, $E_{catalyst}$, and E_{ABS} represent the total energies of the ABS-adsorbed V_2O_5/WO_3-TiO_2 catalyst, pristine V_2O_5/WO_3-TiO_2 catalyst, and isolated ABS molecule, respectively.

3. Results and discussion

3.1. Enhanced activity and sulfur resistance of catalyst with localized vanadia

The catalyst that was mechanochemically synthesized by physically grinding 6 V/DT-52 and DT-52—2 V/DT-52 HL—exhibited physical properties similar to those of conventional 2 V/DT-52. For instance, the vanadia contents and surface areas of 2 V/DT-52 HL and 2 V/DT-52 were almost identical (Table S2). TEM-EDS images acquired at various magnifications showed that the vanadium species in 2 V/DT-52 HL were as well-mixed as those in 2 V/DT-52 (Fig. S2). The in situ Raman spectra of 2 V/DT-52 HL and 2 V/DT-52 were similar (Fig. S3), which confirmed that 6 V/DT-52 and DT-52 were adequately mixed. However, the NH_3-SCR results indicated that 2 V/DT-52 HL exhibited noticeably higher SCR activity than that of 2 V/DT-52 at temperatures below 300 °C (Fig. 1a). For instance, 2 V/DT-52 HL showed an 18% higher NO conversion than that of 2 V/DT-52 at 225 °C. The high activity of 2 V/DT-52 HL could have been caused by the preservation of the highly active vanadyl species of 6 V/DT-52 during the mechanochemical synthesis of 2 V/DT-52 HL. Interestingly, 2 V/DT-52 HL also showed superior resistance to SO_2 poisoning, similar to 2 V/DT-52, whereas the NO_x conversion over 6 V/DT-52 + DT-52 (1:2) decreased continuously owing to SO_2 poisoning (Fig. 1b). It is worth noting that the results of 6 V/DT-52 + DT-52 (1:2)—the catalyst with the same components as those of 2 V/DT-52 HL but not physically ground—are in agreement with previous observations on catalysts with high vanadia surface densities that exhibit high SCR activity, but are susceptible to severe deactivation by SO_2 exposure. Analysis of the SO_2 deactivation rate suggested that 2 V/DT-52 HL was approximately 32% less poisoned than 6 V/DT-52 + DT-52 (1:2) after 10 h of the poisoning test (Fig. 1c). This clearly shows that the physical grinding of 6 V/DT-52 and DT-52 during the synthesis of 2 V/DT-52 HL effectively enhanced the sulfur resistance while maintaining high SCR activity. Therefore, only the advantages of the high- and low-vanadia-loading catalysts—that is, high SCR activity and high sulfur resistance—were obtained by localizing vanadia on the surface of DT-52.

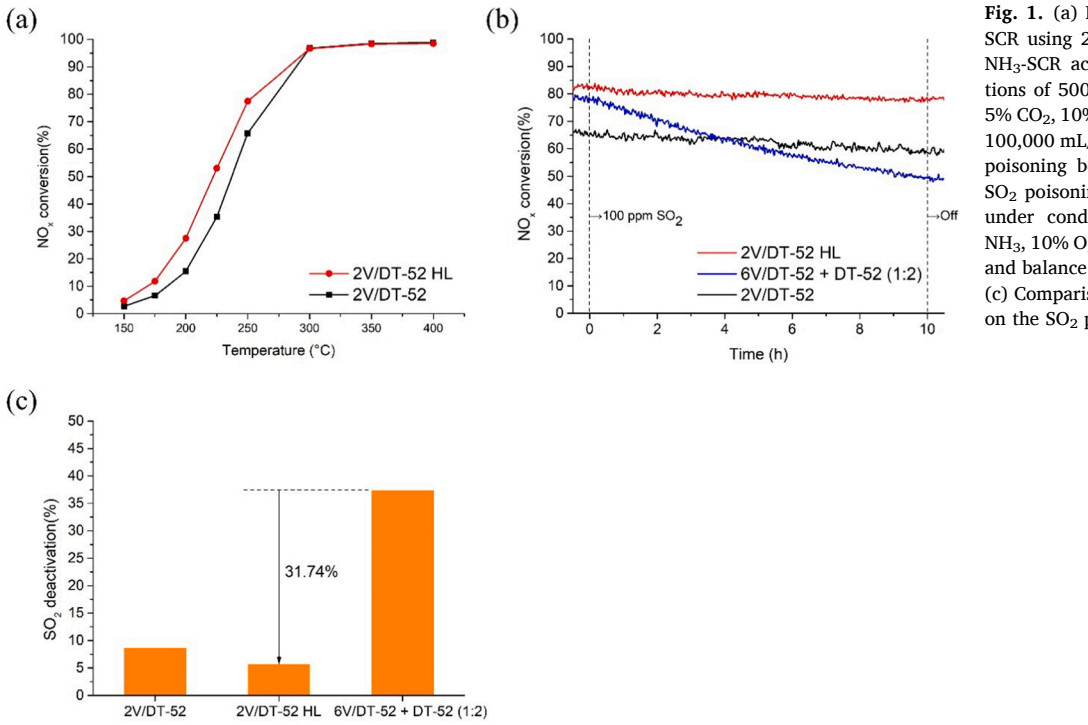

Fig. 1. (a) NO_x conversion achieved via NH_3-SCR using 2 V/DT-52 and 2 V/DT-52 HL. The NH_3-SCR activity was measured under conditions of 500 ppm NO, 600 ppm NH_3, 10% O_2, 5% CO_2, 10% H_2O, and balance N_2 at a GHSV of 100,000 mL/h·g_{cat}. (b) Comparison of SO_2 poisoning behavior of different catalysts. The SO_2 poisoning tests were conducted at 220 °C under conditions of 500 ppm NO, 600 ppm NH_3, 10% O_2, 5% CO_2, 10% H_2O, 100 ppm SO_2, and balance N_2 at a GHSV of 50,000 mL/h·g_{cat}. (c) Comparison of SO_2 deactivation rates based on the SO_2 poisoning tests.

3.2. Structure of vanadia species and its SCR activity

Vanadium with low surface coverage on TiO_2 (<2 V atoms/nm^2) exists primarily as monomeric structures [38,39]. As the vanadium coverage increases, the monomeric vanadyl species transform into polymeric vanadyl species (~2–8 V atoms/nm^2) and crystalline V_2O_5 (>8 V atoms/nm^2) [38,39]. The calculated surface coverages of 2 V/DT-52 and 6 V/DT-52 were 1.51 and 5.47 V atoms/nm^2, respectively. When the TOF of the vanadia species was plotted as a function of the vanadia loading on DT-52 (Fig. 2), the TOF peaked at 6 wt% vanadia loading (that is, 6 V/DT-52), indicating that 6 V/DT-52 had abundant polymeric structures, which are known to be the most active vanadyl structure exhibiting low-temperature NH_3-SCR activity [16]. Moreover,

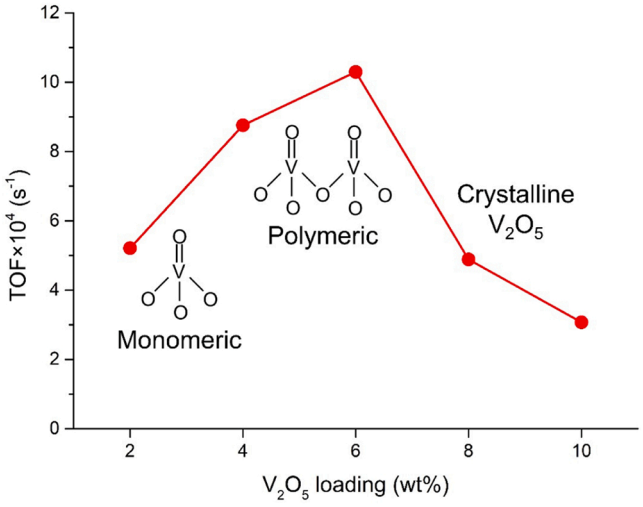

Fig. 2. TOFs for different vanadium species at various vanadia loadings on DT-52. The NH_3-SCR reaction activity was measured at 200 °C under conditions of 500 ppm NO, 600 ppm NH_3, 10% O_2, 5% CO_2, 10% H_2O, and balance N_2. The total flow rate was 200 mL/min, and the GHSV was 600,000 mL/h·g_{cat}. In all cases, NO_x conversions were below 20% to circumvent the diffusion limitation.

these results indicate that the presence of WO_3 on the surface of DT-52 facilitated the formation of the polymeric vanadyl species to a greater degree than that reported previously without WO_3, although the experimental and catalyst preparation conditions do not completely match [40]. The use of higher vanadia loadings than that of 6 V/DT-52 led to the formation of crystalline V_2O_5, as observed in their Raman spectra (Fig. S4), which led to a decrease in their NH_3-SCR activity.

A comparison of the SCR activities monitored during the SO_2-poisoning tests reveals that the initial activity of the 2 V/DT-52 HL catalyst was almost identical to that of 6 V/DT-52 + DT-52 (1:2) (Fig. 1b). Because DT-52 exhibited negligible SCR activity at low temperatures (Fig. S5), the activity of 6 V/DT-52 + DT-52 (1:2 ratio) can be attributed solely to the 6 V/DT-52 particles. If the structure of the vanadia species in 6 V/DT-52 had changed because of the interactions with DT-52 during the synthesis of 2 V/DT-52 HL, the activities of 6 V/DT-52 + DT-52 (1:2) and 2 V/DT-52 HL would have been different. In other words, the similar initial activities indicate that the polymeric vanadia species from 6 V/DT-52 barely changed after undergoing physical grinding with DT-52.

The activation energy results confirmed the preservation of the structure of vanadia after physical mixing (Fig. 3). The activation energy of 2 V/DT-52 was 72.8 kJ/mol, whereas those of 2 V/DT-52 HL and 6 V/DT-52 (58.1 and 59 kJ/mol, respectively) were almost identical. Polymeric vanadia species are known to have a lower overall reaction barrier than that of monomeric vanadia species at low temperatures [16]. Therefore, the aforementioned result strongly corroborates the fact that 2 V/DT-52 HL exhibited catalytic properties of a majority of the polymeric species and adequately preserved the vanadyl structures from the 6 V/DT-52 phase during the physical mixing.

3.3. Comparison between ABS formation and sulfur deactivation

As shown in Fig. 1b, 2 V/DT-52 HL and 6 V/DT-52 + DT-52 (1:2) showed similar initial SCR activities, whereas their sulfur resistances were completely different. To understand the effects of the total amounts of sulfur and ABS on catalyst deactivation, elemental analysis of the SO_2-poisoned samples was performed; the results are listed in

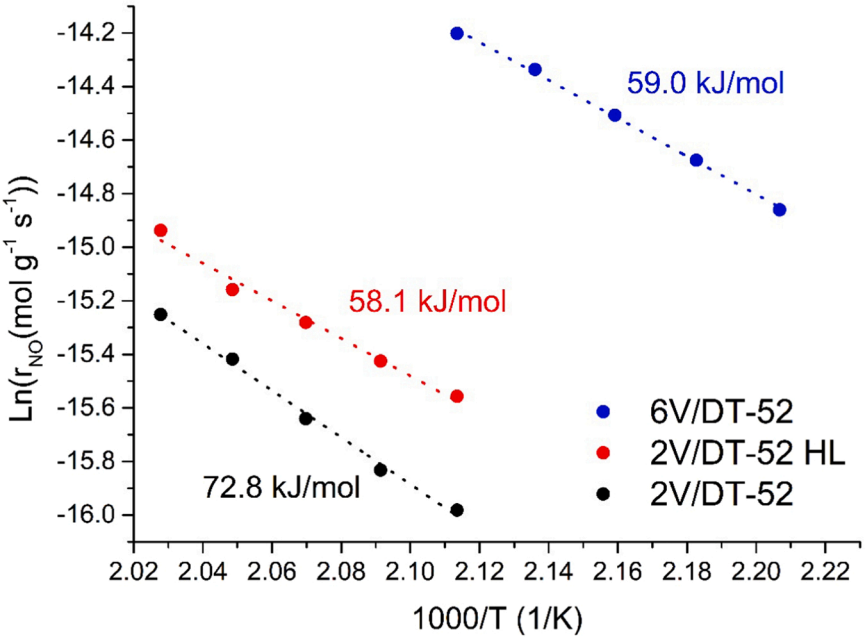

Fig. 3. Arrhenius plots and calculated activation energies of the investigated catalysts. The NH_3-SCR activity was measured under conditions of 500 ppm NO, 600 ppm NH_3, 10% O_2, 5% CO_2, 10% H_2O, and balance N_2. The total flow rate was 200 mL/min, and the GHSV was 600,000 mL/h·g_{cat}. 2 V/DT-52 and 2 V/DT-52 HL were investigated from 200° to 220°C at intervals of 5 °C, whereas 6 V/DT-52 was examined from 180° to 200°C at intervals of 5 °C. In all cases, NO_x conversions were below 20% to ensure that there was no diffusion limitation.

Table S3. Interestingly, the difference in sulfur resistance was not related to the amount of sulfur or ABS formation. Because commercial DT-52 already contains sulfur (0.38 wt%), the ABS amounts were calculated excluding the sulfur already present in the fresh catalysts and by assuming that the increased sulfur content compared to that of the fresh catalysts was entirely converted to ABS. The calculated amounts of ABS in SO_2-poisoned 2 V/DT-52, 6 V/DT-52 + DT-52 (1:2), and 2 V/DT-52 HL were similar. The catalysts underwent SO_2 poisoning for 10 and 20 h, and the corresponding ABS deposition amounts were calculated as 0.6–0.8 wt% per 10 h for all three catalysts.

Because impregnated ABS shows similar characteristics to those of the ABS generated during SO_2 poisoning [41], 1 wt% ABS was impregnated into the fresh catalysts in the present study (based on the Table S3 results), and the SCR activity was determined at 220 °C (Fig. 4). The results of the ABS-impregnated catalysts showed the same tendency as that of the SO_2 poisoning test (Fig. 1). Even with identical amounts of impregnated ABS, 2 V/DT-52 HL showed superior sulfur resistance, similar to 2 V/DT-52, whereas 6 V/DT-52 + DT-52 (1:2) exhibited severely degraded activity after the ABS impregnation. The results of the elemental analysis and SCR tests conducted after the ABS impregnation

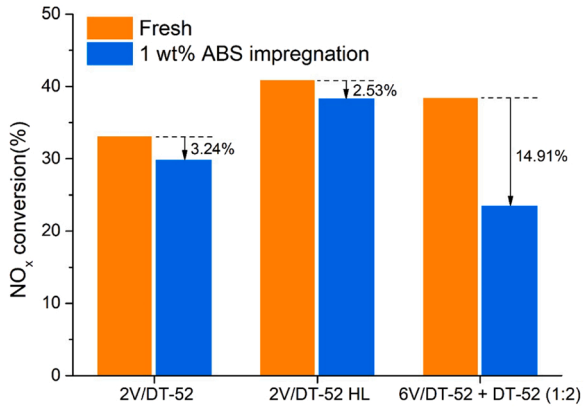

Fig. 4. NO_x conversions achieved via NH_3-SCR using 1-wt%-ABS-impregnated samples. The NH_3-SCR activity was measured at 220 °C for 1 h under conditions of 500 ppm NO, 600 ppm NH_3, 10% O_2, 5% CO_2, 10% H_2O, and balance N_2. The total flow rate was 200 mL/min, and the GHSV was 100,000 mL/h·g_{cat}.

exclude the possibility of the difference in sulfur resistance arising from the amount of ABS formed. Considering that SO_2 oxidation—the key reaction in ABS formation—is dependent on the number of vanadia sites regardless of the vanadia structure, the three catalysts with identical amounts of vanadia presumably formed similar amounts of ABS [13]. The obtained results must be scrutinized further to clarify the superior sulfur (or ABS) resistances of 2 V/DT-52 and 2 V/DT-52 HL compared to those of 6 V/DT-52 + DT-52 (1:2), despite their similar amounts of ABS formed. It is worth noting that the only difference between 2 V/DT-52 HL and 6 V/DT-52 + DT-52 (1:2) was the physical grinding procedure during preparation.

3.4. The origin of sulfur resistance of the catalyst with localized vanadia

The behavior of ABS was investigated to explain the superior sulfur resistance of 2 V/DT-52 HL. Because the melting point of pure ABS is 147 °C, ABS exists as a viscous liquid at operating temperatures below 300 °C. ABS in sticky liquid form physically interacts with the catalyst surface, blocking the pores and active sites [8]. Previous studies by our group have revealed that liquid-phase ABS can migrate to the surface of vanadia catalysts [32–34]. Essentially, the ABS that is initially formed on the surface of V_2O_5/WO_3-TiO_2 migrates to physically connected zeolite or alumina surfaces, thereby protecting the vanadia active sites of V_2O_5/WO_3-TiO_2 from ABS deactivation [32–34]. A similar ABS migration could also occur on the surface of 2 V/DT-52 HL.

ABS (2 wt%) was pre-impregnated into 6 V/DT-52 to monitor the migration of ABS; the resulting product is denoted as 2ABS-6 V/DT-52. The processes used for preparing 2 V/DT-52 HL and 6 V/DT-52 + DT-52 (1:2) were repeated using 2ABS-6 V/DT-52 instead of fresh 6 V/DT-52; the synthesis schemes of the resulting catalysts (denoted as (2ABS-V)− 2 V/DT-52 HL and 2ABS-6 V/DT-52 + DT-52 (1:2), respectively) are shown in Fig. S6a for clarity. The two ABS-impregnated samples were heated to 220 °C at a ramping rate of 1.5 °C/min under the NH_3-SCR conditions. Although ABS was equally impregnated on the vanadia sites in both samples, the activity of 2ABS-6 V/DT-52 + DT-52 (1:2) was noticeably deactivated by ABS, whereas that of (2ABS-V)− 2 V/DT-52 HL was hardly affected, as it showed a profile that was almost identical to that of fresh 2 V/DT-52 HL (Fig. S6b). To conduct a more comprehensive analysis, Arrhenius plots were obtained based on the NO_x conversion results acquired at temperatures of 140–220 °C (Fig. 5). The

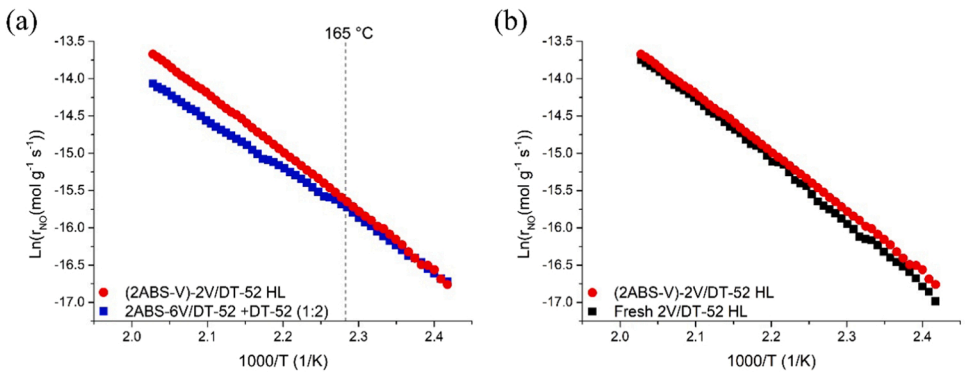

Fig. 5. Arrhenius plot of (2ABS-V)− 2 V/DT-52 HL compared with those of (a) 2ABS-6 V/DT-52 + DT-52 (1:2) and (b) 2 V/DT-52 HL during transient NH_3-SCR. The NH_3-SCR activity was measured under conditions of 500 ppm NO, 600 ppm NH_3, 10% O_2, 5% CO_2, 10% H_2O, and balance N_2. The total flow rate was 200 mL/min, and the GHSV was 100,000 mL/h·g_{cat}. The conversion was measured from 100° to 220°C with a ramping rate of 1.5 °C/min. The NO_x conversion profiles are shown in Fig. S6.

Arrhenius plots of (2ABS-V)− 2 V/DT-52 HL, 2ABS-6 V/DT-52 + DT-52 (1:2), and fresh 2 V/DT-52 HL were almost identical at temperatures below 165 °C, indicating that solid-phase ABS did not deactivate the catalysts [32]. However, at temperatures above 165 °C, where ABS presumably melts into a liquid phase on the V_2O_5/WO_3-TiO_2 surface, the slope of 2ABS-6 V/DT-52 + DT-52 (1:2) started to decrease, whereas that of (2ABS-V)− 2 V/DT-52 HL was maintained at the same value as that of fresh 2 V/DT-52 HL. In other words, liquid-phase ABS severely deactivated 2ABS-6 V/DT-52 + DT-52 (1:2), but barely deactivated (2ABS-V)− 2 V/DT-52 HL. This phenomenon can be explained by ABS migration. The movement of ABS from 6 V/DT-52 to DT-52 in the 6 V/DT-52 + DT-52 (1:2) catalyst is unlikely, as 6 V/DT-52 and DT-52 were pelletized and sieved separately. Therefore, in the case of 6 V/DT-52 + DT-52 (1:2), ABS covered the vanadia active sites when it melted at temperatures above 165 °C, thereby deactivating the catalyst. In contrast, the ABS on the vanadia sites of 2 V/DT-52 HL migrated as a liquid at this temperature, which restored the vanadia active sites. This result is in line with previous observations made by our group, in which a similar Arrhenius plot tendency was noted when the ABS impregnated on V_2O_5/WO_3-TiO_2 migrated as a liquid to physically mixed zeolite on top, with the plot diverging at temperatures above 160 °C [32]. Therefore, this result suggests that the mobile ABS liquid formed on the vanadia active sites in 2 V/DT-52 HL possibly migrated to the physically mixed DT-52.

The local distributions of the SO_2-poisoned catalysts were determined by TEM-EDS analysis to verify the ABS migration model. The results (Fig. 6a–d) demonstrate that the distribution of ABS corresponded with the distribution of vanadium species in 6 V/DT-52 + DT-52 (1:2), thereby confirming ABS formation on the vanadia sites. The distribution of sulfur in the 2 V/DT-52 HL sample was not proportional to the distribution of vanadium (Fig. 6e, f). This result corroborates the migration of ABS, which was initially formed on the vanadium sites, to the vanadium-free WO_3-TiO_2 support.

Other materials such as silica and DT-51 were tested to investigate the role of the physically ground DT-52 in ABS migration. The results of the sulfur resistance tests and TEM-EDS analysis of 2 V/DT-52 HL-Silica and 2 V/DT-52 HL-DT-51 are shown in Figs. S7 and S8, respectively. Although the specific surface area of fumed silica (395 m^2/g) was approximately four times higher than that of DT-52 (93 m^2/g), 2 V/DT-52 HL-Silica showed poor sulfur resistance, similar to 6 V/DT-52 + DT-52 (1:2 ratio) (Fig. S7a, b). In terms of the TEM-EDS results, sulfur only existed in the 6 V/DT-52 region, and the migration of ABS to silica was not observed (Fig. S7c, d). This result indicates that the ABS migration in 2 V/DT-52 HL was not a common phenomenon of mass diffusion to high-surface-area materials.

The surface of DT-52 provided both WO_3 and exposed TiO_2 sites. The calculated surface coverage of WO_3 is 2.13 atoms/nm^2, which is less than half the monolayer coverage of WO_3 (4.5 atoms/nm^2) [42,43]. Thus, 2 V/DT-52 HL-DT-51 was tested to determine whether WO_3 sites or exposed TiO_2 sites were responsible for the ABS migration. Although only TiO_2 sites were provided by grinding DT-51, the 2 V/DT-52 HL-DT-51 sample showed a sulfur deactivation rate identical to that of 2 V/DT-52 HL (Fig. S8). Additionally, previous studies have shown that direct adsorption of ABS on TiO_2 is extremely favorable, whereas that on WO_3 is not preferred [44]. Overall, these results suggest that the addition of exposed TiO_2 sites was strongly responsible for ABS migration in the investigated system, regardless of the presence of WO_3. Excluding WO_3 in the catalytic system, 2 V/DT-51 HL was also approximately 30% less deactivated than 6 V/DT-51 + DT-51 (1:2), further corroborating that WO_3 has a negligible role in ABS migration (Fig. S9).

The physical grinding of DT-52 presumably provided a more stable environment for ABS than that on the vanadia active sites of 6 V/DT-52 for migration of ABS from the vanadia active sites. TPD analysis was performed for the ABS-impregnated and SO_2-poisoned samples to compare the stability of ABS on the catalysts by detecting desorbed SO_2 (Fig. 7). TiO_2 supports are known to collapse at high temperatures (>600 °C). Small desorption peaks of SO_2 appeared at temperatures above 600 °C, which can be assigned to the decomposition of inherent TiO_2 sulfate in DT-52. The coverage of vanadia species, even at low loadings, impedes the formation of surface titania sulfate species [45]. Therefore, additional formation of titania sulfate in the vanadia catalysts was negligible, allowing this study to focus on the ABS peaks below 600 °C.

1ABS-DT-52 exhibited an ABS decomposition peak at a high temperature of 542 °C (Fig. 7a). Moreover, the decomposition peak temperature of ABS on 1ABS-DT-51 (~550 °C) was similar to that of 1ABS-DT-52. This implies that the influence of WO_3 on the stability of ABS in DT-52 was negligible. When vanadia was loaded onto DT-52, the decomposition peak shifted to a notably lower temperature. The peak temperature of 1ABS-2 V/DT-52 was 459 °C. The intensity of the ABS decomposition peak of 1ABS-6 V/DT-52 decreased further to 426 °C with increasing vanadia loading, which is consistent with previously reported results [41,46]. Therefore, the coverage of vanadia on DT-52 evidently made ABS less stable and enabled its decomposition at a lower temperature.

The SO_2 peak of SO_2-poisoned 6 V/DT-52 + DT-52 (1:2) appeared at 431 °C, which corresponded to the peak of 1ABS-6 V/DT-52 (Fig. 7b). The decomposition peak of SO_2-poisoned 2 V/DT-52 HL appeared at 456 °C, which suggests that the TiO_2 sites added by grinding DT-52 clearly provided a more stable environment for the ABS. SO_2-poisoned 2 V/DT-52 HL did not exhibit a decomposition peak at 542 °C, which was observed in 1ABS-DT-52. This implies that the TiO_2 species in 2 V/DT-52 HL were well mixed and different from those on the surface of bare DT-52. Furthermore, the similar peak temperatures of 2 V/DT-52 HL (~456 °C) and 2 V/DT-52 (~467 °C) suggest that the added TiO_2 sites made the surface of 2 V/DT-52 HL similar to that of 2 V/DT-52 for permitting ABS–catalyst interactions and ABS desorption.

The surface environment of 2 V/DT-52 HL was investigated further to understand the dispersion of the TiO_2 species. The NH_3-TPD results for DT-51 and various loadings of V/DT-52 are presented in Fig. S10a.

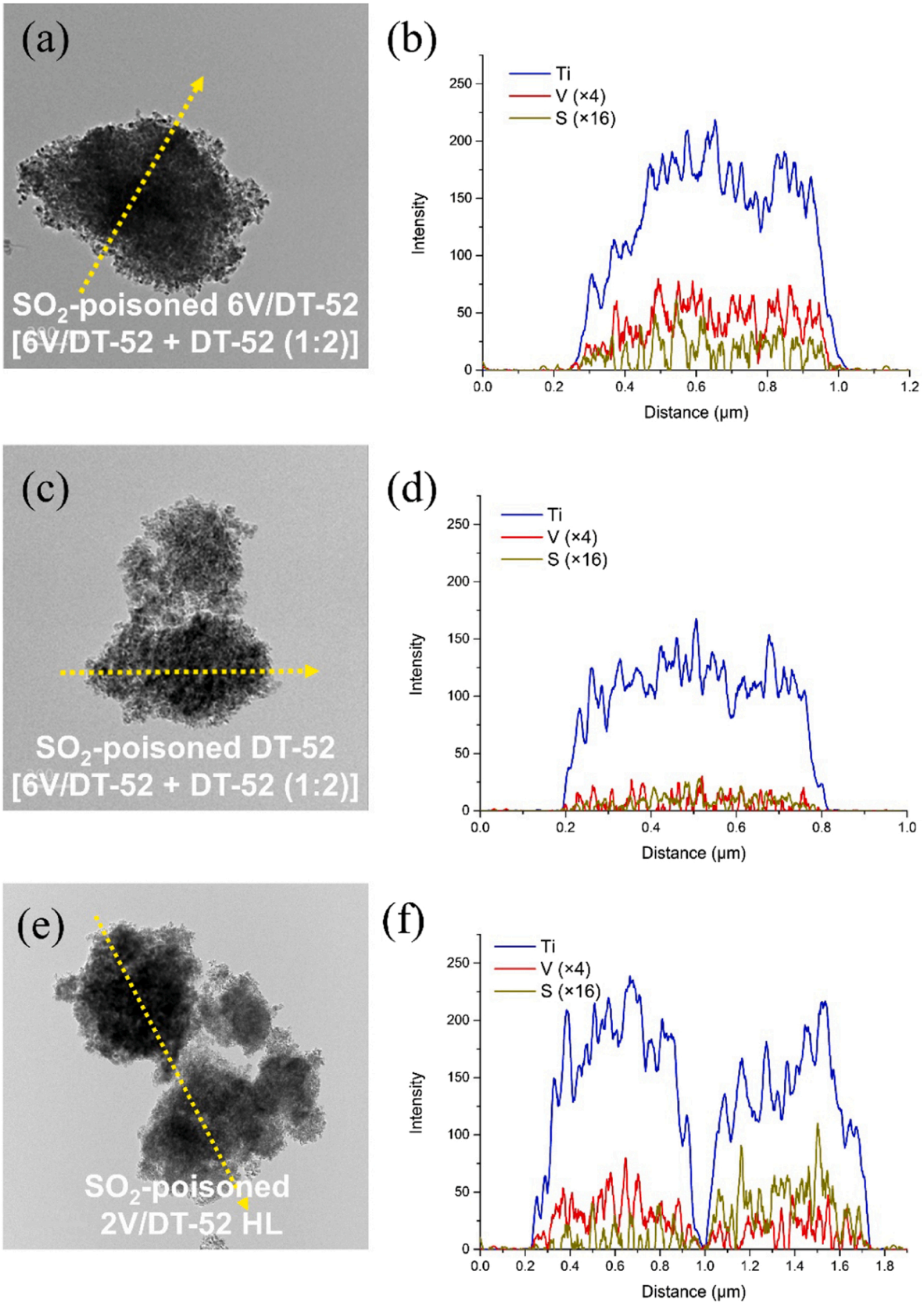

Fig. 6. TEM images and line-EDS profiles of Ti, V, and S in (a, b) SO_2-poisoned 6 V/DT-52 from the 6 V/DT-52 + DT-52 (1:2) catalyst, (c, d) SO_2-poisoned DT-52 from the 6 V/DT-52 + DT-52 (1:2) catalyst, and (e, f) SO_2-poisoned 2 V/DT-52 HL. The sieved particles of 6 V/DT-52 and DT-52 in the 6 V/DT-52 + DT-52 (1:2) sample were distinguishable by color and separated manually.

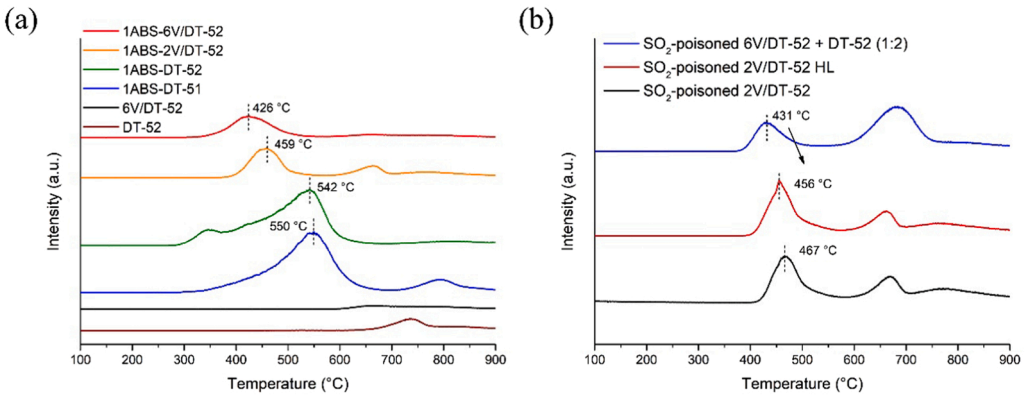

Fig. 7. TPD profiles of (a) 1-wt%-ABS-impregnated, fresh, and (b) SO_2-aged catalysts detecting SO_2. N_2 was used with a GHSV of 60,000 mL/h·g_{cat}, and the temperature was increased from 100° to 900°C with a ramping rate of 10 °C/min.

Compared to DT-51, DT-52 shows a small peak around 500 °C which arises from strong acid sites formed by surface W^{6+} species [47]. At low vanadia loadings on the surface of DT-52, surface-exposed Ti^{4+} Lewis acid sites adjacent to vanadyl species are presumed to generate a peak at high temperatures (>400 °C) [47–49]. As the vanadia loading increased, the peak intensity gradually decreased and the NH_3 desorption peak shifted to lower temperatures. However, the NH_3 desorption peak was not clearly visible in the NH_3-TPD result for 6 V/DT-52, indicating that the surface of 6 V/DT-52 was fully covered with vanadia species without exposed TiO_2 sites. Interestingly, the mechanochemically prepared 2 V/DT-52 HL showed a similar NH_3 desorption temperature and peak intensity to those of 2 V/DT-52 (Fig. 8). The NH_3-adsorption spectra acquired via DRIFTS supported the NH_3-TPD results (Fig. S10b). The NH_3 peak at 1243 cm^{-1}, which can be assigned to Lewis acid sites, was observed in the profiles of 2 V/DT-52 HL, 2 V/DT-52, and DT-52, but not in that of 6 V/DT-52 [50,51]. The NH_3 peak at 1428 cm^{-1}, which can be assigned to Brønsted acid sites, increased in intensity in the order DT-52, 2 V/DT-52, 2 V/DT-52 HL, and 6 V/DT-52 [50,51]. The NH_3-TPD and NH_3-DRIFTS results indicate that the physical grinding of 6 V/DT-52 and DT-52 generated exposed TiO_2 sites adjacent to the vanadyl species, similar to the sites of 2 V/DT-52 created using the wetness impregnation method. This generation of TiO_2 sites adjacent to vanadyl species by physical grinding was possible presumably because of the characteristics of DT-52, which is not a porous material. TEM and SEM images indicated the particles of DT-52 were extremely small (~25 nm) and interacted extensively with each other, forming closely packed clusters (Fig. 9). Therefore, most of the DT-52 surface was covered with other DT-52 particles locating the vanadia active sites at the interparticle interfaces. The TEM-EDS images shown in Fig. S2 indicate that 2 V/DT-52 HL was mixed at the particle level. The highly intimate interface between the DT-52 and 6 V/DT-52 particles in the 2 V/DT-52 HL catalyst likely acted as TiO_2 sites adjacent to the vanadyl species in 2 V/DT-52.

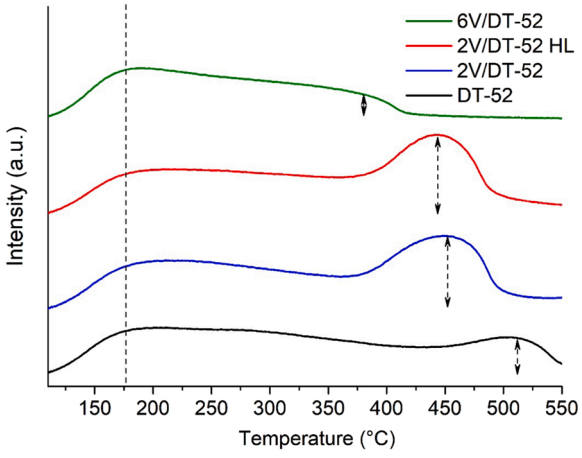

Fig. 8. NH_3-TPD results for 6 V/DT-52, 2 V/DT-52 HL, 2 V/DT-52 and DT-52 with different vanadia loadings.

To gain a deeper understanding of the role of adjacent exposed TiO_2 sites on ABS migration, the ABS adsorption energies at various sites of V_2O_5/WO_3-TiO_2 were calculated using DFT (Table 1, Fig. 10, and Fig. S11). The adsorption energy was calculated for two cases: (1) ABS directly adsorbed onto the surface of vanadium or tungsten species, and (2) ABS adsorbed onto exposed TiO_2 species adjacent to vanadium or tungsten species. The adsorption energy of the most stable configuration was calculated for each case. The calculated energy for direct adsorption of ABS onto vanadyl or tungsten species was extremely low (−0.2 to −0.35 eV) because the repulsion of vanadyl or tungsten species against the sulfate species of ABS hindered the adsorption (Table 1 and Fig. 10) [44,52]. However, regardless of the vanadyl structure, when the sulfate species moved to the adjacent exposed TiO_2 sites, ABS was noticeably stabilized, which increased the adsorption energy (−0.77 to −1.45 eV). This result explains the temperature difference between the SO_2-poisoned 6 V/DT-52 + DT-52 (1:2) and SO_2-poisoned 2 V/DT-52 HL samples observed in the SO_2-TPD analysis. The supply of adjacent TiO_2 sites caused the sulfate species of ABS to move away from the vanadia species, which increased the stability of ABS. This migration protected the vanadia active sites and SO_2-stability of 2 V/DT-52HL during the NH_3-SCR reaction. Based on these characterization results, the sulfur resistance mechanism in V_2O_5-WO_3/TiO_2 can be explained by simply using the model of ABS migration to exposed adjacent TiO_2 species. High-vanadia-loading catalysts do not have exposed TiO_2 sites for enabling the movement of ABS. This causes the newly formed ABS to directly block the vanadia active sites without moving to other sites (that is, TiO_2 in DT-52), which severely hampers the NH_3-SCR activity of vanadia sites in the presence of SO_2. Low-vanadia-loading catalysts maintain strong sulfur resistance at low temperatures because ABS preferentially moves from the vanadia active sites to adjacent TiO_2 sites. The sulfur resistance of the vanadia catalysts is related to the TiO_2 sites adjacent to the vanadia species, regardless of the vanadia structure. It is worth noting that these adjacent TiO_2 sites could be generated by simply grinding TiO_2, which highlights the potential of mechanochemical synthesis to simultaneously provide polymeric species and exposed TiO_2 sites, thereby enhancing both sulfur resistance and SCR activity.

4. Conclusion

The biotoxicity of V_2O_5 and the dilemma related to the use of high vanadia loadings that leads to rapid ABS deactivation have led to the commercialization of low-vanadia-loading V_2O_5/WO_3-TiO_2 catalysts,

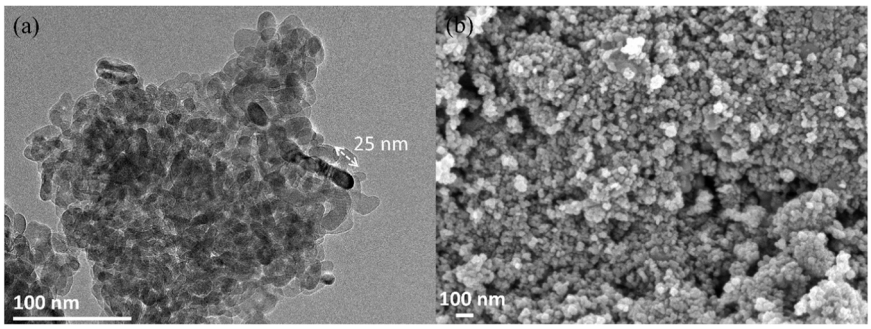

Fig. 9. (a) TEM and (b) SEM images of 2 V/DT-52 HL. The TEM image was acquired after the catalyst was highly dispersed using acetone.

Table 1
DFT-calculated adsorption energies of ABS on various sites of V_2O_5/WO_3-TiO_2.

Structure	Adsorption Energy (eV)	
	Direct adsorption	With exposed adjacent TiO_2
Monomeric VO_3	− 0.346	− 1.445
Polymeric V_2O_5	− 0.287	− 0.860
VWO_5	− 0.264	− 0.775
Monomeric WO_3	− 0.204	− 1.119

despite their inferior NH_3-SCR activity at low temperatures. However, the NH_3-SCR activity correlated with the structure of vanadia, and the sulfur resistance dependent on the exposure of TiO_2 was not a trade-off relationship. High NH_3-SCR activity and sulfur resistance were simultaneously achieved in this study by physically grinding high-vanadia-loaded V_2O_5/WO_3-TiO_2 with WO_3-TiO_2. On the surface of the mechanochemically prepared catalysts, clustered vanadia species enhanced the SCR activity by forming polymeric structures. The physical grinding generated exposed TiO_2 sites adjacent to the vanadia active sites, which absorbed liquid-phase ABS, resulting in superior sulfur resistance even at high SCR activity. A comprehensive investigation of the ABS adsorption energy at different sites in the V_2O_5/WO_3-TiO_2 catalysts further revealed the role of exposed TiO_2 sites that were adjacent to vanadia on the high sulfur resistance of low-vanadia-loading catalysts, which has not been suggested before.

CRediT authorship contribution statement

Keon Ha Hwang: Conceptualization, Validation, Investigation, Writing – original draft, Writing – review & editing, Visualization. **Namjun Park:** Software, Investigation. **Hwangho Lee:** Investigation, Writing – review & editing. **Kyung-Min Lee:** Investigation, Writing – review & editing. **Se Won Jeon:** Writing – review & editing. **Hyun Sub**

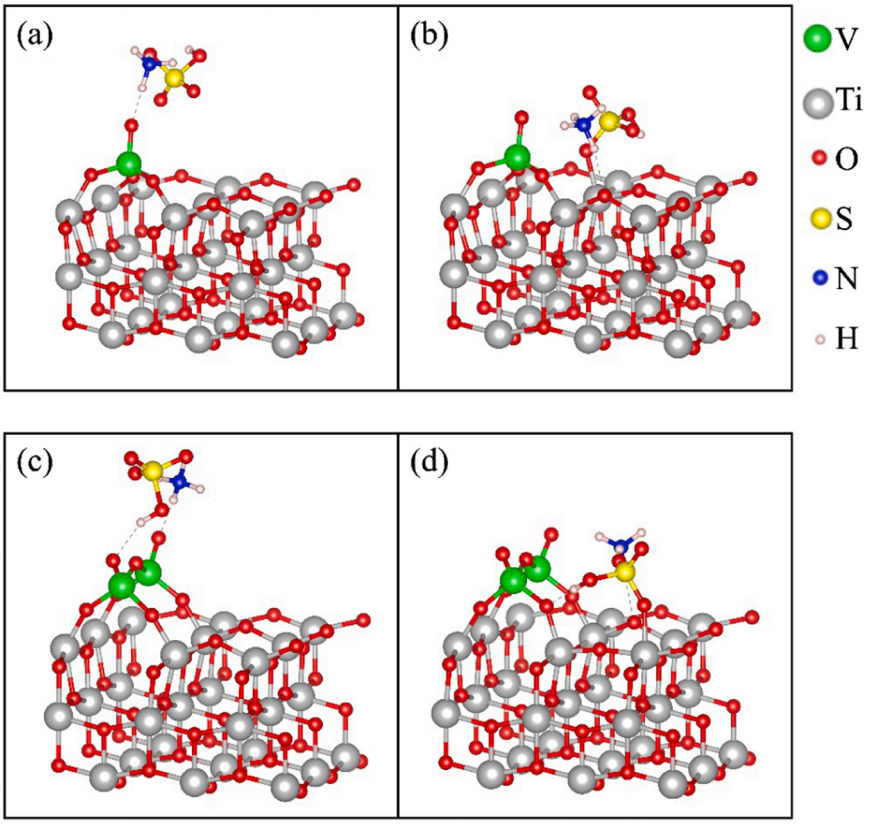

Fig. 10. DFT-generated schematics of ABS adsorption on (a) monomeric VO_3, (b) exposed TiO_2 adjacent to monomeric VO_3, (c) polymeric V_2O_5, and (d) exposed TiO_2 adjacent to polymeric V_2O_5 (green, V atoms; gray, Ti atoms; red, O atoms; yellow, S atoms; blue, N atoms; and white, H atoms). The adsorption of ABS onto other structures is shown in Fig. S11.

Kim: Writing – review & editing. **Yongkyu Lee:** Software, Investigation. **Tae Jin Kim:** Investigation, Writing – review & editing. **Won Bo Lee:** Software, Writing – review & editing. **Do Heui Kim:** Supervision, Funding acquisition, Writing – review & editing.

Declaration of Competing Interest

The authors declare that they have no known competing financial interests or personal relationships that could have appeared to influence the work reported in this paper.

Data Availability

Data will be made available on request.

Acknowledgments

This study was supported by Basic Science Research Programs (grant nos. NRF-2022R1A2C3013253 and NRF-2016R1A5A1009592) through the National Research Foundation of Korea (NRF), funded by the Ministry of Science and ICT and the Ministry of Science, ICT & Future Planning (MSIP), respectively. The research facilities at the Institute of Engineering Research at Seoul National University were employed for this study.

Appendix A. Supporting information

Supplementary data associated with this article can be found in the online version at doi:10.1016/j.apcatb.2022.122290.

References

[1] L. Han, S. Cai, M. Gao, J.-y Hasegawa, P. Wang, J. Zhang, L. Shi, D. Zhang, Selective catalytic reduction of NO_x with NH_3 by using novel catalysts: state of the art and future prospects, Chem. Rev. 119 (2019) 10916–10976.
[2] W. Shan, H. Song, Catalysts for the selective catalytic reduction of NO_x with NH_3 at low temperature, Catal. Sci. Technol. 5 (2015) 4280–4288.
[3] Y. Huo, K. Liu, J. Liu, H. He, Effects of SO_2 on standard and fast SCR over $CeWO_x$: a quantitative study of the reaction pathway and active sites, Appl. Catal. B: Environ. 301 (2022), 120784.
[4] E. Park, M. Kim, H. Jung, S. Chin, J. Jurng, Effect of sulfur on Mn/Ti catalysts prepared using chemical vapor condensation (CVC) for low-temperature NO reduction, ACS Catal. 3 (2013) 1518–1525.
[5] J. Li, H. Chang, L. Ma, J. Hao, R.T. Yang, Low-temperature selective catalytic reduction of NO_x with NH_3 over metal oxide and zeolite catalysts—a review, Catal. Today 175 (2011) 147–156.
[6] L. Gan, K. Li, W. Yang, J. Chen, Y. Peng, J. Li, Core-shell-like structured α-MnO_2@CeO_2 catalyst for selective catalytic reduction of NO: promoted activity and SO_2 tolerance, Chem. Eng. J. 391 (2020), 123473.
[7] H. Lee, R.J.G. Nuguid, S.W. Jeon, H.S. Kim, K.H. Hwang, O. Kröcher, D. Ferri, D. H. Kim, In situ spectroscopic studies of the effect of water on the redox cycle of Cu ions in Cu-SSZ-13 during selective catalytic reduction of NO_x, Chem. Commun. 58 (2022) 6610–6613.
[8] K. Guo, J. Ji, W. Song, J. Sun, C. Tang, L. Dong, Conquering ammonium bisulfate poison over low-temperature NH_3-SCR catalysts: a critical review, Appl. Catal. B: Environ. 297 (2021), 120388.
[9] Y. Inomata, S. Hata, M. Mino, E. Kiyonaga, K. Morita, K. Hikino, K. Yoshida, H. Kubota, T. Toyao, K.-i Shimizu, M. Haruta, T. Murayama, Bulk vanadium oxide versus conventional V_2O_5/TiO_2: NH_3–SCR catalysts working at a low temperature below 150 °C, ACS Catal. 9 (2019) 9327–9331.
[10] W.H.J. Graus, E. Worrell, Effects of SO_2 and NO_x control on energy-efficiency power generation, Energy Policy 35 (2007) 3898–3908.
[11] X. Wang, X. Du, S. Liu, G. Yang, Y. Chen, L. Zhang, X. Tu, Understanding the deposition and reaction mechanism of ammonium bisulfate on a vanadia SCR catalyst: A combined DFT and experimental study, Appl. Catal. B: Environ. 260 (2020), 118168.
[12] L. Muzio, S. Bogseth, R. Himes, Y.-C. Chien, D. Dunn-Rankin, Ammonium bisulfate formation and reduced load SCR operation, Fuel 206 (2017) 180–189.
[13] J.P. Dunn, P.R. Koppula, H.G. Stenger, I.E. Wachs, Oxidation of sulfur dioxide to sulfur trioxide over supported vanadia catalysts, Appl. Catal. B: Environ. 19 (1998) 103–117.
[14] B. Ye, B. Jeong, M.-j Lee, T.H. Kim, S.-S. Park, J. Jung, S. Lee, H.-D. Kim, Recent trends in vanadium-based SCR catalysts for NOx reduction in industrial applications: stationary sources, Nano Converg. 9 (2022) 51.
[15] Z.G. Liu, N.A. Ottinger, C.M. Cremeens, Vanadium and tungsten release from V-based selective catalytic reduction diesel aftertreatment, Atmos. Environ. 104 (2015) 154–161.
[16] G. He, Z. Lian, Y. Yu, Y. Yang, K. Liu, X. Shi, Z. Yan, W. Shan, H. He, Polymeric vanadyl species determine the low-temperature activity of V-based catalysts for the SCR of NO_x with NH_3, Sci. Adv. 4 (2018), eaau4637.
[17] J.M. Won, M.S. Kim, S.C. Hong, Effect of vanadium surface density and structure in VO_x/TiO_2 on selective catalytic reduction by NH_3, Korean J. Chem. Eng. 35 (2018) 2365–2378.
[18] D.W. Kwon, K.B. Nam, S.C. Hong, The role of ceria on the activity and SO_2 resistance of catalysts for the selective catalytic reduction of NO_x by NH_3, Appl. Catal. B: Environ. 166–167 (2015) 37–44.
[19] M. Guo, B. Mosevitzky Lis, M.E. Ford, I.E. Wachs, Effect of redox promoters (CeO_x and CuO_x) and surface sulfates on the selective catalytic reduction (SCR) of NO with NH_3 by supported V_2O_5-WO_3/TiO_2 catalysts, Appl. Catal. B: Environ. 306 (2022), 121108.
[20] M.S. Maqbool, A.K. Pullur, H.P. Ha, Novel sulfation effect on low-temperature activity enhancement of CeO_2-added Sb-V_2O_5/TiO_2 catalyst for NH_3-SCR, Appl. Catal. B: Environ. 152–153 (2014) 28–37.
[21] D.W. Kwon, D.H. Kim, S. Lee, J. Kim, H.P. Ha, A dual catalytic strategy by the nature of the functionalization effect as well as active species on vanadium-based catalyst for enhanced low temperature SCR, Appl. Catal. B: Environ. 289 (2021), 120032.
[22] M. Guo, B. Mosevitzky Lis, M.E. Ford, I.E. Wachs, The effect of non-redox promoters (AlO_x, PO_x, SiO_x and ZrO_x) and surface sulfates on supported V_2O_5-WO_3/TiO_2 catalysts in selective catalytic reduction of NO with NH_3, Appl. Catal. B: Environ. 306 (2022), 121128.
[23] X. Huang, G. Zhang, G. Lu, Z. Tang, Recent progress on establishing structure–activity relationship of catalysts for selective catalytic reduction (SCR) of NO_x with NH_3, Catal. Surv. Asia 22 (2018) 1–19.
[24] J.-K. Lai, N.R. Jaegers, B.M. Lis, M. Guo, M.E. Ford, E. Walter, Y. Wang, J.Z. Hu, I. E. Wachs, Structure–activity relationships of hydrothermally aged titania-supported vanadium–tungsten oxide catalysts for SCR of NO_x emissions with NH_3, ACS Catal. 11 (2021) 12096–12111.
[25] J. Cao, W. Liu, K. Kang, L. Chen, X. Qiao, X. Yao, Effects of the morphology and crystal-plane of TiO_2 on NH_3-SCR performance and K tolerance of V_2O_5-WO_3/TiO_2 catalyst, Appl. Catal. A: Gen. 623 (2021), 118285.
[26] T. Friščić, C. Mottillo, H.M. Titi, Mechanochemistry for synthesis, Angew. Chem. Int. Ed. 59 (2020) 1018–1029.
[27] A.P. Amrute, Z. Łodziana, H. Schreyer, C. Weidenthaler, F. Schüth, High-surface-area corundum by mechanochemically induced phase transformation of boehmite, Science 366 (2019) 485–489.
[28] M. Bilke, P. Losch, O. Vozniuk, A. Bodach, F. Schüth, Methane to chloromethane by mechanochemical activation: a selective radical pathway, J. Am. Chem. Soc. 141 (2019) 11212–11218.
[29] S. Ndayiragije, Y. Zhang, Y. Zhou, Z. Song, N. Wang, T. Majima, L. Zhu, Mechanochemically tailoring oxygen vacancies of MnO_2 for efficient degradation of tetrabromobisphenol A with peroxymonosulfate, Appl. Catal. B: Environ. 307 (2022), 121168.
[30] H. Schreyer, R. Eckert, S. Immohr, J. DeBellis, M. Felderhoff, F. Schüth, Milling down to nanometers: a general process for the direct dry synthesis of supported metal catalysts, Angew. Chem. Int. Ed. 58 (2019) 11262–11265.
[31] J. Ji, Y. Tang, L. Han, P. Ran, W. Song, Y. Cai, W. Tan, J. Sun, C. Tang, L. Dong, Cerium manganese oxides coupled with ZSM-5: A novel SCR catalyst with superior K resistance, Chem. Eng. J. 445 (2022), 136530.
[32] I. Song, H. Lee, S.W. Jeon, I.A.M. Ibrahim, J. Kim, Y. Byun, D.J. Koh, J.W. Han, D. H. Kim, Simple physical mixing of zeolite prevents sulfur deactivation of vanadia catalysts for NO_x removal, Nat. Commun. 12 (2021) 901.
[33] S.W. Jeon, I. Song, H. Lee, J. Kim, Y. Byun, D.J. Koh, D.H. Kim, Enhanced SO_2 resistance of V_2O_5/WO_3-TiO_2 catalyst physically mixed with alumina for the selective catalytic reduction of NO_x with NH_3, Chem. Eng. J. 433 (2022), 133836.
[34] I. Song, S.W. Jeon, H. Lee, D.H. Kim, Tailoring the mechanochemical interaction between vanadium oxides and zeolite for sulfur-resistant DeNO_x catalysts, Appl. Catal. B: Environ. 316 (2022), 121672.
[35] G. Kresse, J. Furthmüller, Efficient iterative schemes for ab initio total-energy calculations using a plane-wave basis set, Phys. Rev. B 54 (1996) 11169–11186.
[36] J.P. Perdew, K. Burke, M. Ernzerhof, Generalized gradient approximation made simple, Phys. Rev. Lett. 77 (1996) 3865–3868.
[37] A. Suarez Negreira, J. Wilcox, Role of WO_3 in the Hg oxidation across the V_2O_5–WO_3–TiO_2 SCR catalyst: a DFT study, J. Phys. Chem. C 117 (2013) 24397–24406.
[38] J.-K. Lai, I.E. Wachs, A perspective on the selective catalytic reduction (SCR) of NO with NH_3 by supported V_2O_5–WO_3/TiO_2 catalysts, ACS Catal. 8 (2018) 6537–6551.
[39] H. Tian, E.I. Ross, I.E. Wachs, Quantitative determination of the speciation of surface vanadium oxides and their catalytic activity, J. Phys. Chem. B 110 (2006) 9593–9600.
[40] N.R. Jaegers, J.K. Lai, Y. He, E. Walter, D.A. Dixon, M. Vasiliu, Y. Chen, C. Wang, M.Y. Hu, K.T. Mueller, I.E. Wachs, Y. Wang, J.Z. Hu, Mechanism by which tungsten oxide promotes the activity of supported V_2O_5/TiO_2 catalysts for NO_x abatement: structural effect, Angew. Chem. 131 (2019) 12739–12746.
[41] D. Ye, R. Qu, H. Song, X. Gao, Z. Luo, M. Ni, K. Cen, New insights into the various decomposition and reactivity behaviors of NH_4HSO_4 with NO on V_2O_5/TiO_2 catalyst surfaces, Chem. Eng. J. 283 (2016) 846–854.
[42] D.S. Kim, M. Ostromecki, I.E. Wachs, Surface structures of supported tungsten oxide catalysts under dehydrated conditions, J. Mol. Catal. A: Chem. 106 (1996) 93–102.

[43] T. Kim, A. Burrows, C.J. Kiely, I.E. Wachs, Molecular/electronic structure–surface acidity relationships of model-supported tungsten oxide catalysts, J. Catal. 246 (2007) 370–381.
[44] J. Yu, E. Zhang, L. Wang, Z. Song, F. Kong, Y. Ma, H. Zhao, L. Sun, The interaction of NH_4HSO_4 with vanadium–titanium catalysts modified with molybdenum and tungsten, Energy Fuels 34 (2020) 2107–2116.
[45] M.D. Amiridis, I.E. Wachs, G. Deo, J.-M. Jehng, D.S. Kim, Reactivity of V_2O_5 catalysts for the selective catalytic reduction of NO by NH_3: influence of vanadia loading, H_2O, and SO_2, J. Catal. 161 (1996) 247–253.
[46] R. Qu, D. Ye, C. Zheng, X. Gao, Z. Luo, M. Ni, K. Cen, Exploring the role of V_2O_5 in the reactivity of NH_4HSO_4 with NO on V_2O_5/TiO_2 SCR catalysts, RSC Adv. 6 (2016) 102436–102443.
[47] M. Zhu, J.-K. Lai, U. Tumuluri, Z. Wu, I.E. Wachs, Nature of Active Sites and Surface Intermediates during SCR of NO with NH_3 by Supported V_2O_5–WO_3/TiO_2 Catalysts, J. Am. Chem. Soc. 139 (2017) 15624–15627.
[48] I. Song, J. Lee, G. Lee, J.W. Han, D.H. Kim, Chemisorption of NH_3 on Monomeric Vanadium Oxide Supported on Anatase TiO_2: s Combined DRIFT and DFT Study, J. Phys. Chem. C 122 (2018) 16674–16682.
[49] M. Gallastegi-Villa, A. Aranzabal, M.P. González-Marcos, B.A. Markaide-Aiastui, J. A. González-Marcos, J.R. González-Velasco, Effect of vanadia loading on acidic and redox properties of VO_x/TiO_2 for the simultaneous abatement of PCDD/Fs and NO_x, J. Ind. Eng. Chem. 81 (2020) 440–450.
[50] I. Song, H. Lee, S.W. Jeon, D.H. Kim, Understanding the dynamic behavior of acid sites on TiO_2-supported vanadia catalysts via operando DRIFTS under SCR-relevant conditions, J. Catal. 382 (2020) 269–279.
[51] R.J.G. Nuguid, L. Ortino-Ghini, V.L. Suskevich, J. Yang, L. Lietti, O. Kröcher, D. Ferri, Interconversion between Lewis and Brønsted–Lowry acid sites on vanadia-based catalysts, Phys. Chem. Chem. Phys. 24 (2022) 4555–4561.
[52] S.T. Choo, Y.G. Lee, I.-S. Nam, S.-W. Ham, J.-B. Lee, Characteristics of V-$_2O_5$ supported on sulfated TiO_2 for selective catalytic reduction of NO by NH_3, Appl. Catal. A: Gen. 200 (2000) 177–188.